Research Article

Shape tunability of carbonized cellulose nanocrystals

Mattia Bartoli[1] · Mauro Giorcelli[1] · Pravin Jagdale[2] · Massimo Rovere[1] · Alberto Tagliaferro[1,3] · Michael Chae[4] · David C. Bressler[4]

Received: 25 September 2019 / Accepted: 19 November 2019 / Published online: 23 November 2019

Abstract
Bioderived scaffolds are largely used as template for the synthesis of drugs and materials. Among biomass sources, cellulose has been used as platform for numerous conversions and applications. In this study, we report the use of crystalline microstructured cellulose as feedstock for microstructured carbon production. Different morphologies were produced according to pyrolytic conditions ranging from sphere, needle and carbon-on-carbon-decorated surfaces. All the materials were characterized using spectroscopic techniques (i.e., Raman, FTIR), FESEM and thermogravimetric analysis. Hypothetical reaction pathways were proposed for describing materials shape and properties. In particular, for cellulose nanocrystals, the thermal treatments induced noteworthy electrical properties that could be applied for the production of conductive composites.

Keywords Cellulose nanocrystals · Carbon spheres · Carbon needles · Pyrolysis · Carbon tailoring

1 Introduction

Cellulose is the most abundant constituent of lignocellulosic biomass [1] and one of the most common utilized feedstocks for biorefinery platforms and processes [2, 3]. Cellulose nanocrystals (CNCs) are a very interesting material derived by cellulose chemical [4] or enzymatic [5] controlled hydrolysis of different sources [6, 7]. Pristine CNCs show remarkably high storage modulus together with a very attractive aspect ratio [8]. Additionally, CNCs are characterized by an interesting polymorphism induced by tailoring with inorganic or organic functionalities [9–11]. This behavior was particularly relevant in the related composites where polymorphic CNCs induced very different properties [12, 13]. Despite these usefully properties, pristine CNCs lack in conductivity and dispersibility in nonpolar media [14, 15]. Also, pristine CNCs show the tendency to self-assemble into aggregates driven by strong hydrogen bond network formation [16]. As reported by Beck et al. [17], in the dried solid state CNCs are aggregated as round-shaped structures with an average size ranging from 10 to 20 µm. These drawbacks slow down their application in polymer composite science requiring the use of plasticizers [18, 19] or chemical modifications [20] for an efficient use. Alternatively, thermochemical CNCs conversion routes have been studied using the CNCs structures as templates for the production of nano- and microstructured carbonaceous materials such as carbon nanodots [21]. The interest for micro- and nanostructured carbon has grown over the years since the discovery of allotropic carbon species (i.e., carbon nanotubes, fullerene) and carbon fibers [22]. Nano- and microstructured carbon materials have gained

Electronic supplementary material The online version of this article (https://doi.org/10.1007/s42452-019-1727-2) contains supplementary material, which is available to authorized users.

✉ Mattia Bartoli, mattia.bartoli@polito.it | [1]Department of Applied Science and Technology, Polytechnic of Turin, C.so Duca degli Abruzzi 24, 10129 Turin, Italy. [2]Center for Sustainable Future, Italian Institute of Technology, Via Livorno 60, 10144 Turin, Italy. [3]Faculty of Science, University of Ontario Institute of Technology, 2000 Simcoe Street North, Oshawa, ON, Canada. [4]Department of Agricultural, Food and Nutritional Science, University of Alberta, 410 Ag/For Building, Edmonton, AB T6G 2P5, Canada.

great attention for energy harvesting [23] and energy storage applications [24, 25]. Cellulose has been proved a very promising template for the production of carbonaceous materials [26–28]. CNCs are good candidates as feedstock in nanostructured carbon production as demonstrated by Wu et al. [29]. Authors used a CNCs/melamine resin precursor to produce nitrogen-enriched nanorods used for energy storage devices production, achieving remarkable performance. Shopsowitz et al. [30] described a similar methodology producing carbonized nematic material using CNCs and silica. Furthermore, the use of a CNCs/organic polymer precursor was used to produce micro-carbon fibers [31, 32]. Chou et al. [33] reported a multi-step protocol for the conversion of commercial microcrystalline cellulose into carbonized fibers on nanoscale using the freeze drying technique. Recently, Eom et al. [34] described the graphitization process of CNCs from 1000 to 2500 °C using spray pyrolysis methodology to obtain fiber structures. Moreover, rounded carbon particles have been successfully used for water purification and environmental remediation [35, 36], composites production [37, 38] and energy storage [39]. According to the great interest in the carbon shape tunability, we used CNCs as template for producing microstructured carbon species, ranging from spherical to needle-like structures. We investigated the shape tunability of carbonized CNCs using solid-state and dispersed CNCs using several temperatures (400 °C, 600 °C, 800 °C, 1000 °C). The carbonaceous materials produced were studied using field emission scanning electron microscopy, spectroscopic and thermal techniques to evaluate their main properties. Carbon tailoring tunability will represent the first step for further studies focused on the reinforced polymers. The nanosized tailoring could be a winning factor for the enhancement of mechanical properties improving the interactions between the polymeric matrix and the carbonaceous filler avoiding the use of additional inorganic tailoring [40, 41].

2 Materials and methods

2.1 Materials

CNCs were purchased from Alberta-Pacific Forest Industries (Batch COMP170823-H) and used as received without any purification. Ethanol (EtOH, 98%) and polyethylene glycol (PEG, molecular weight 200 g/mol) were purchased by Sigma-Aldrich and used without any purification.

2.2 Carbonization of CNCs

Pyrolysis experiments were carried out using 25 g of CNCs. CNCs were placed in a ceramic crucible and then introduced into a quartz reactor. The reactor was sealed and a flux of argon was used to remove the initial residual atmosphere. The argon flux (4 mL/min) was kept constant during the pyrolytic run to drag out the gas released by the thermal degradation reactions. The heating rate was set at 50 °C/min with a set high treatment temperature (HTT), respectively, of 400 °C, 600 °C, 800 °C and 1000 °C. The system was kept at the HTT for 30 min and fast cooled down at room temperature using refrigerated water in argon atmosphere.

Subsequently, 25 g of CNCs were dispersed into 250 mL of water, EtOH or PEG through 10-min mechanical mix. The reactor was sealed and a flux of argon was used to remove the initial residual atmosphere. The argon flux was kept constant during the pyrolytic run. The reactor was placed in a preheated oven at 800 °C or 1000 °C. After an initial temperature decrease, the system rapidly came back to the preset temperature and it was left at HTT for 30 min. After that, it was fast cooled down at room temperature using refrigerated water in argon atmosphere.

2.3 Methods

Morphology of all samples was investigated using a field emission scanning electrical microscope (FESEM, Zeiss Supra 40). Pristine CNCs were coated with 5 µm layer of chromium prior the analysis to enhance the resolution. The metallic film deposition was performed using sputtering technique.

Carbonized CNCs were analyzed using Fourier transform infrared (FTIR) spectroscope (FTIR Nicolet 5700, Thermo Scientific) equipped with a SmartOrbit (Thermo Scientific) operating in attenuated total reflectance (ATR) in a range between 500 and 4000 cm^{-1}.

Furthermore, Raman spectroscopy was used to investigate the carbon produced using a Renishaw® Ramanscope InVia (H43662) model equipped with a green laser source. The Raman spectra in a range from 250 to 3300 cm^{-1} were fitted with homemade software developed using MATLAB™ in order to fit the component peaks.

Stability of carbonaceous materials was investigated through thermogravimetric analysis (TGA) using Netzsch TG 209F1 Libra in N_2 flux with a temperature ramp of 10 °C/min from 30 to 900 °C.

Conductivity measurements were taken with the method described by Giorcelli et al. [42] using a hydraulic press (Specac Atlas Manual Hydraulic Press 15T) and multimeter (Agilent 34401A). (A briefly description is reported

in Scheme 1 of supporting materials.) Resistance of carbonized CNCs was measured applying a pressure ranging from 1 to 1500 bar. Conductivity was calculated according to the following equation:

$$\sigma = R\left(\frac{l}{A}\right) \quad (1)$$

where σ is the conductivity of the carbonized material, R is the measured resistance, A is the bottom surface of the copper cylinder and l is the thickness of the carbonized material.

3 Results

3.1 Yields of CNCs pyrolytic run

CNCs were carbonized using temperatures ranging from 400 to 1000 °C. This temperature range covers all the main degradative stages of cellulose [43, 44] together with the main stages of biochar evolution [45]. As shown in Fig. 1, the increment of temperature depleted the carbonized CNCs yields from 26.3 ± 0.8 wt% at 400 °C to 14.1 ± 1.0 at 1000 °C as reported by many authors [45, 46].

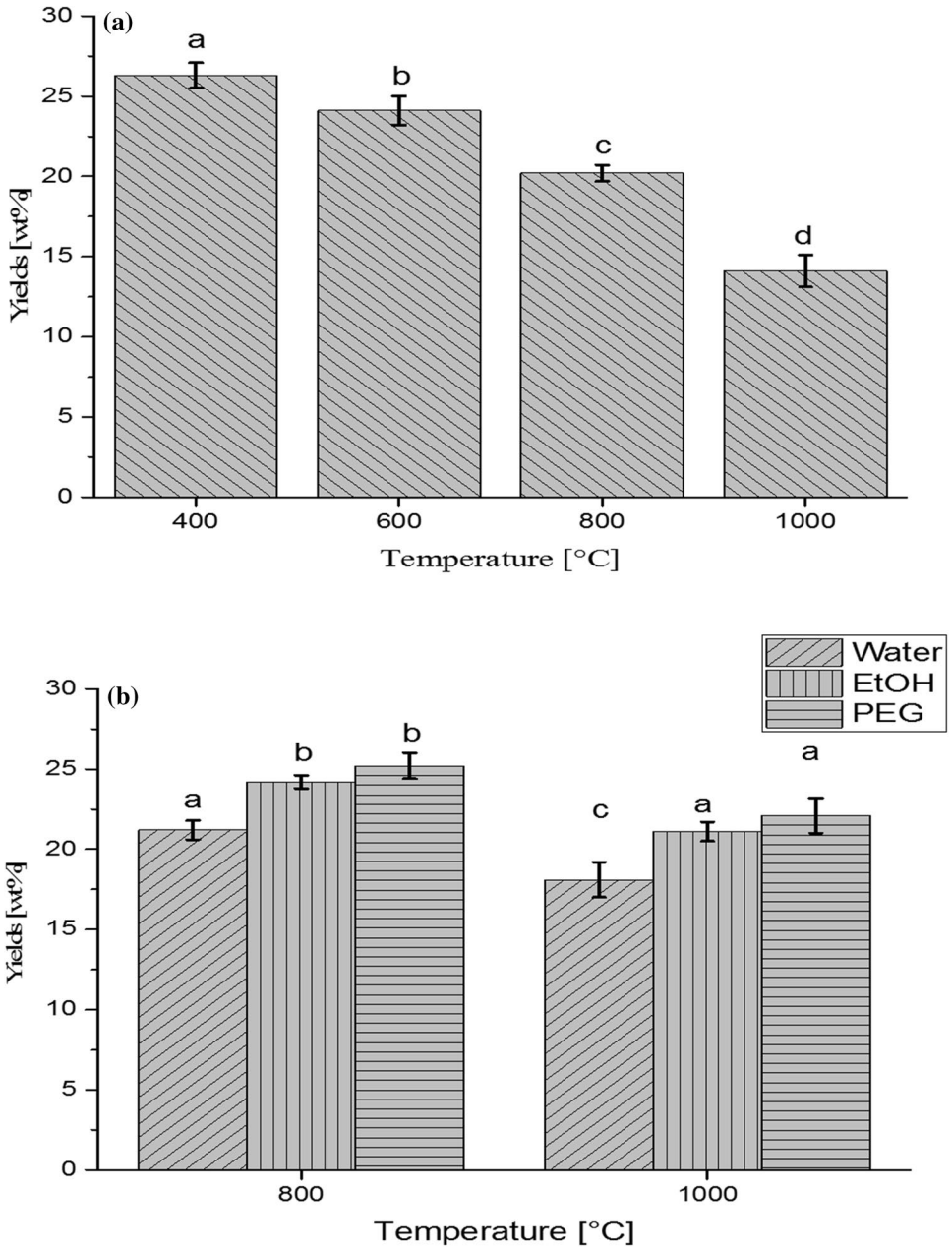

Fig. 1 Yields of pyrolysis of solid state form CNCs (**a**) and CNCs solvent dispersed (**b**) at different temperatures. Data were reported as average values of three runs with error bars representing the standard deviation. Data marked with same letters are not significantly different ($p < 0.05$)

As reported by Buffa et al. [47], the rheology of the CNCs dispersion is very sensitive to the addition of additives and polarity of the medium chosen. Room-temperature dispersion of CNCs is commonly achieved using polar solvents such as water [48], alcohols [49] or polyethers as non-ion surfactants [50]. The use of solvents during pyrolysis under pressure is a common practice to promote more homogenous reaction conditions [51]. We selected water as the simplest polar solvent, and we studied how the increment of unpolar residues using EtOH and PEG affected the pyrolytic behavior of CNCs dispersions according to the interactions proposed in Fig. 2.

In this study, solvents were rapidly removed of degraded during pyrolysis run. In these experiments, an initial temperature decrease was observed reaching 850–800 °C and 650–630 °C using a preheated furnace at 1000 °C and 800 °C, respectively. The temperature was rapidly increased to the original value, while the solvent was removed.

The use of water as a solvent did not significantly affect the yield (21.2 ± 0.6 wt%) of recovered carbonized CNCs at 800 °C and promoted an appreciable yield increment at 1000 °C, achieving 18.1 ± 1.1 wt%. This was reasonably due to the partial suppression of levoglucosan formation due to the watery residual atmosphere with a decrease in formation of highly reactive species such as hydroxyfurfural. Using EtOH or PEG, an increase in the yields was observed at both 800 °C (24.2 ± 0.4 wt% and 25.2 ± 0.8 wt%) and 1000 °C (21.1 ± 0.6 wt% and 22.1 ± 1.1 wt%). This appreciable increment was probably due to the radical simultaneous degradation of organic solvent used as reaction medium together with pristine CNCs.

3.2 FESEM analysis of carbonized CNCs

Pristine CNCs were analyzed using FESEM (Fig. 3) after chromium metallization.

Pristine CNCs were aggregated as defective spheres with average diameters ranging from 2 to 10 µm. Spheroidal particles formed an interconnected network (Fig. 2b) kept together by hydrogen bonds [52]. Contrary, nanometric-sized CNCs were observed using dispersed material in very low concentration as described by many authors [5, 53, 54].

The FESEM images collected after pyrolysis of pristine CNCs at different temperatures are shown in Fig. 4.

All the images collected show a partial retention of the initial structure with some defects on the surfaces (magnified in Fig. 5) due to the release of volatile organic matter during pyrolysis. In the early stages of the thermal degradation of the CNCs, pyrolysis of the sphere surface took place simultaneously with the release of the high-boiling compounds (levoglucosan, glucose dimers and trimers [55]) from the inner particle cores. After reaching the surface, these compounds started to boil and to decompose at the same time. The results of this process are the tiny bubbles clearly visible in Fig. 4 and magnified in Fig. 5.

Other noteworthy needle structures were observed using HTT up to 600 °C in Fig. 4; they are more clearly visible in Fig. 5b–d.

The needle structures showed a remarkable aspect ratio considering the length of 1–3 µm, a width around 200 nm and a negligible thickness.

Focusing the probe of the FESEM, the needles degradation was observed proving their carbon-based structure (Supporting Information Figure 1).

The carbonized CNCs lost their spherical shape after water was used as a solvent medium (Fig. 6).

Needle structures were detected in large amounts in the shape of carbon needles (Fig. 6a) as either isolated needles or regrouped into clusters (Fig. 6b). This could be explained by the presence of water that could induce the pyrolytic degradation of the partially unpacked CNCs in the early stages of the process.

An increment of pyrolytic temperature to 1000 °C leads to decrement of the amount of carbon needles (Fig. 6d). Furthermore, the increased temperature promoted an excessively fast evaporation of the solvent avoiding the formation of clearly separated needles.

A different behavior was observed using EtOH as a solvent medium (Fig. 7).

Applying a pyrolytic temperature of 800 °C, EtOH-dispersed CNCs retained the spherical structure of packed pristine CNCs (Fig. 7a) even when the surfaces were massively decorated with hemispheres (Fig. 7b). This behavior could be ascribed to the very fast evaporation and simultaneous degradation of EtOH that competed with pyrolytic degradation of dispersed CNCs. Further temperature increase to 1000 °C induced the formation of needle clusters as shown in Fig. 7c, d. This could be explained with the same arguments above mentioned considering watery medium. The high temperature promoted a very fast evaporation of EtOH, but at 1000 °C the temperature of the system was high enough to induce simultaneously the degradation of CNCs, leading to the formation of carbon needles. The use of PEG induced the collapse of any structures to amorphous materials (Fig. 8a, c). This was the degradation of PEG during the pyrolysis that substantially enriched the radical concentration. Adopting a processing temperature of 800 °C, PEG could be used to decorate the surface of carbonized CNCs with pyramidal structures with an average size of 100 nm (Fig. 8b), while a smooth surface was obtained at 1000 °C (Fig. 8d).

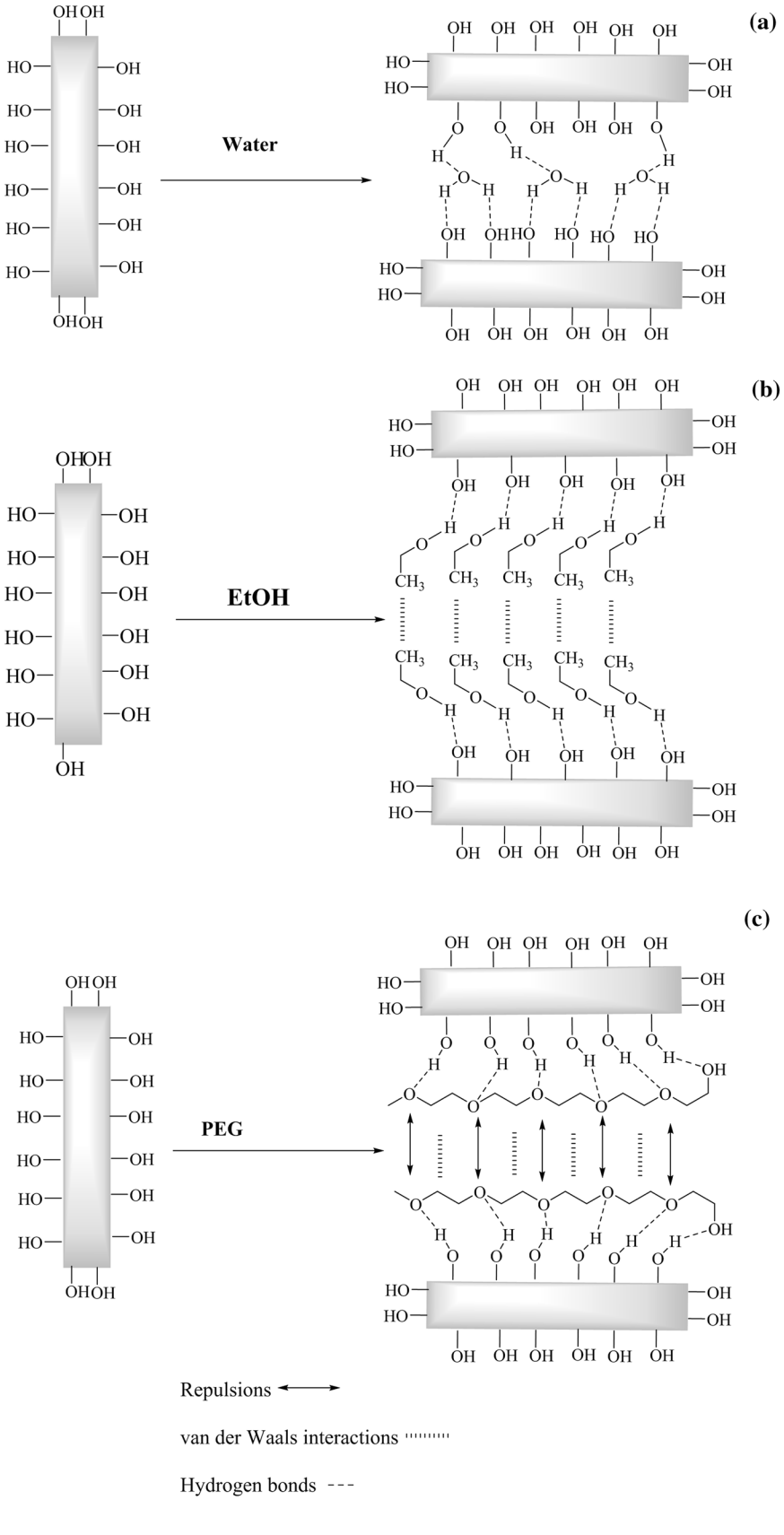

Fig. 2 Hypothetical interaction of solvent-dispersed CNCs: **a** water, **b** EtOH and **c** PEG

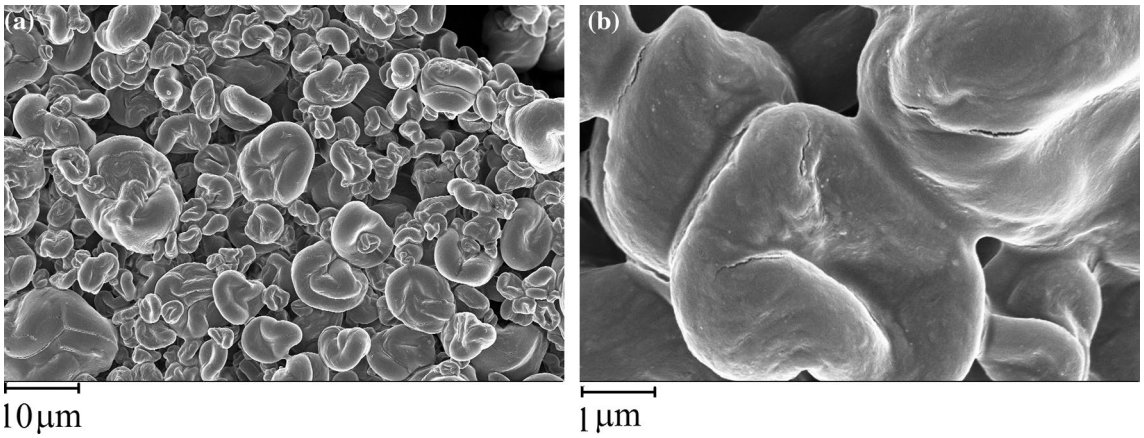

Fig. 3 FE-SEM capture of **a** pristine CNCs and **b** surface details after metallization

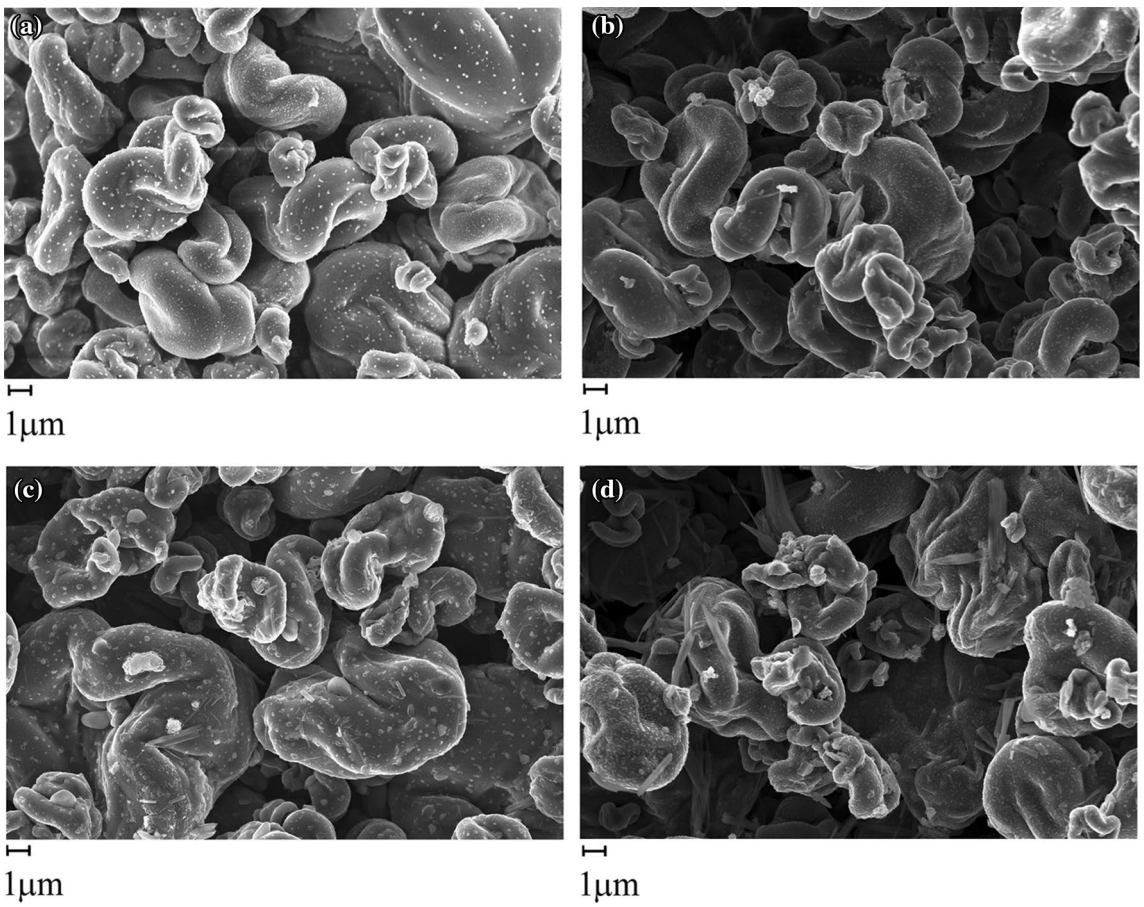

Fig. 4 FE-SEM images of carbonized CNCs at 400 °C (**a**), 600 °C (**b**), 800 °C (**c**) and 1000 °C (**d**)

3.3 Spectroscopic analysis on carbonized CNCs

Raman analysis is a very powerful tool to analyze carbonaceous materials [56]. As reported by Ferrari et al. [57], Raman spectroscopy can be used to evaluate the disorder of amorphous carbon using the area ratio of D and G peaks. Raman spectra of carbonized CNCs are reported in Fig. 9 and show D and G peaks centered, respectively, at 1346–1371 cm^{-1} and 1590 cm^{-1}.

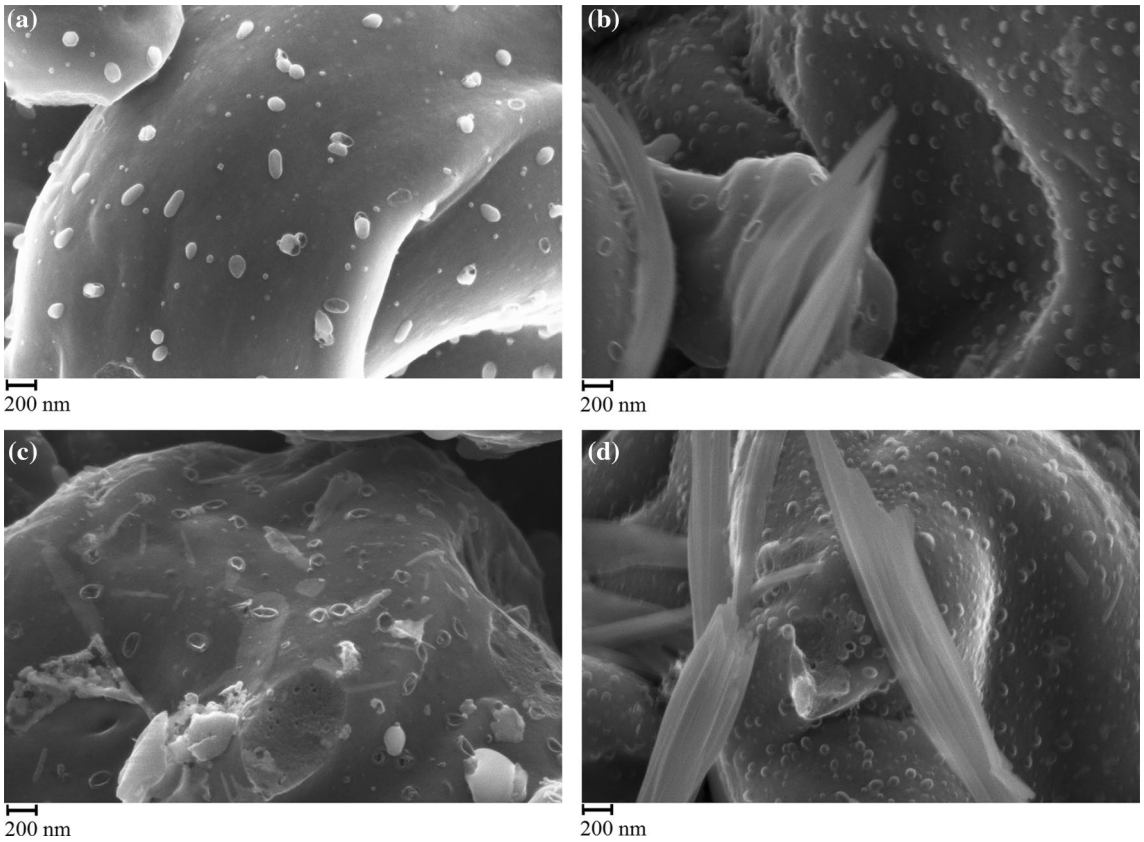

Fig. 5 Surface details of CNCs pyrolyzed at 400 °C (**a**), 600 °C (**b**), 800 °C (**c**) and 1000 °C (**d**)

Based on I_D/I_G ratio, pyrolyzed CNCs without the addition of solvents show an increase in disorder moving from HTT of 400–600 °C. Further increments of HTT (800 °C and 1000 °C) induced a carbon structure reorganization due to the increase in and enlargement of aromatic domains.

As shown in Fig. 10, CNCs pyrolyzed using solvents showed an appreciable increment of I_D/I_G with a more disordered structure produced when PEG was used. For a HTT of 1000 °C h, trend was less relevant remaining only an appreciable difference in the saddle of the carbonized PEG-dispersed CNCs.

Pristine and carbonized CNCs were analyzed through FTIR (ATR mode), and representative spectra are reported in Fig. 11.

Pristine CNCs spectrum (Fig. 11c) showed a broad band between 3600 and 3300 cm^{-1} due to the presence of hydroxylic groups (ν_{O-H}), signals of saturated ν_{C-H} at 2900–2850 cm^{-1}, ν_{CH2} at 1426 cm^{-1} due to the C6 of glucose structure and a band envelopment between 900 and 1100 cm^{-1} due to the δ_{CH2} and ν_{C-O}. As a consequence of the first acidic hydrolysis, CNCs also showed a low intense peak at 1205 cm^{-1} ($\nu_{S=O}$) due to sulfate residual groups. The literature lacks of study about sulfonated cellulose pyrolysis, but several authors described the effect of sulfonated additives able to enhance dehydration pathways to anhydrosugars and furans [58, 59]. According to these studies, it is possible to assume that the sulfate functionalities affected more biooils than biochar production. Nonetheless, they play a relevant role in a solvent-assisted pyrolytic process inducing a better dispersibility.

The spectrum of carbonized CNCs at 400 °C (Fig. 11b) did not show any bands at 3600 or 2850 cm^{-1} according to the pyrolytic degradation of cellulose chains [60]. Some residual groups could be detected such as ketonic (1580 cm^{-1}, $\nu_{C=O}$) and carboxylic ($\nu_{C=O}$ at 1700 cm^{-1} and ν_{O-H} at 1436 cm^{-1}) functionalities together with ethers (ν_{C-O} at 1228 cm^{-1} and δ_{C-O} at 1119 cm^{-1}). A further increment of HTT to 600 °C (Fig. 11 a) leads to the total loss of surface functionalities caused by the advanced thermal degradation reactions. Similar results were observed at higher HTT (800 °C, 1000 °C) with or without the use of a solvent medium. The absence of relevant IR signals proved the complete absence of EtOH or PEG residues.

3.4 Conductivity measurements of carbonized CNCs

Conductivity measurements on CNCs were performed using a hydraulic press that trough two copper cylinders

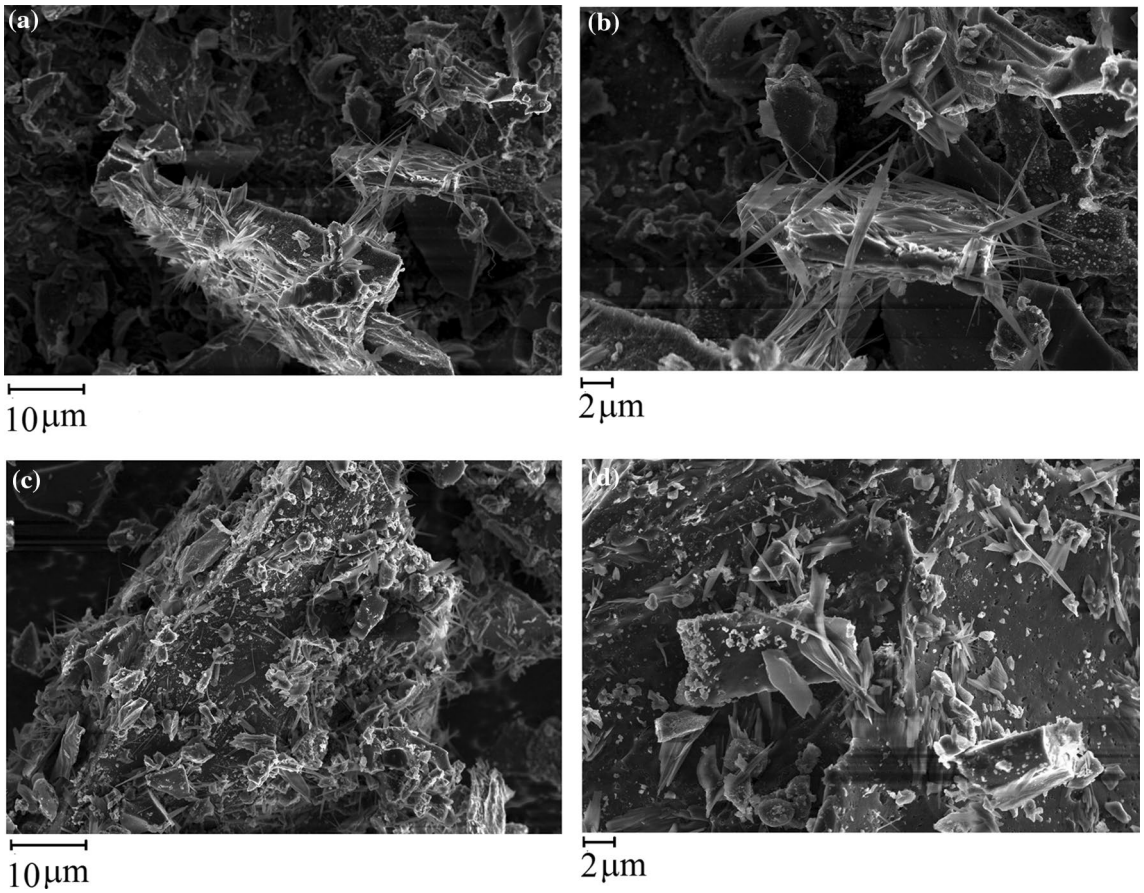

Fig. 6 FE-SEM images of carbonized CNCs watery solution at 800 °C (**a** and **b**) and 1000 °C (**c** and **d**)

measure the resistance variation during the compression (Supporting Information Scheme 1), and results are shown in Fig. 12.

Carbonized CNCs at 400 °C showed an insulator behavior up to a pressure of 300 bar, while carbonized CNCs at 600 °C showed higher values reaching a value around 7 S/m at 400 bar. It was impossible to measure a reliable conductivity values for all samples obtained at 800 °C and 1000 °C because they were indistinguishable from the reference. Relation between conductivity and temperature was described by Giorcelli et al. [42] using pristine and thermally annealed biochar applied for composite production. The increment of conductivity was due to the formation and the turbostratic reorientation of graphitic domains in the carbon matrix [61, 62]. Formation of small graphitic domains was also supported by the disappearing of the IR signals after treatments up to 600 °C (Fig. 11a). At higher temperatures, these domains become bigger and ordered with layered graphitic structures [34]. According to Ferrari et al. [57], the transition phase from amorphous to nanocrystalline graphite carbon could be monitored through the shift of I_G peak position from low to higher Raman shift. CNCs pyrolyzed at 400 °C showed an I_G peak at 1580 cm^{-1}, while the CNCs peak showed an I_G peak at 1593 cm^{-1} close to the full nanocrystalline graphite carbon at 1600 cm^{-1}. Furthermore, this process was also associated with a disorganization of the material in good agreement with the increment of I_D/I_G ratio observed in the spectra reported in Fig. 9.

The monolithic biochar showed conductivity around 10 S/m [63], and consequently, the well-packed materials above described showed a good improvement of up one or two orders of magnitude.

3.5 Thermogravimetric analysis of carbonized CNCs

All carbonized CNCs were analyzed using thermogravimetric analysis (TGA). In Fig. 13 are reported the results of pristine and carbonized CNCs.

Thermal stability of carbonized CNCs was strongly affected by thermal history of the material. Pristine CNCs show a 5 wt% loss at 101 °C due to water loss and a main degradation process around 250 °C primarily due to the breakage of β-1,4-glycosidic bonds of the cellulosic

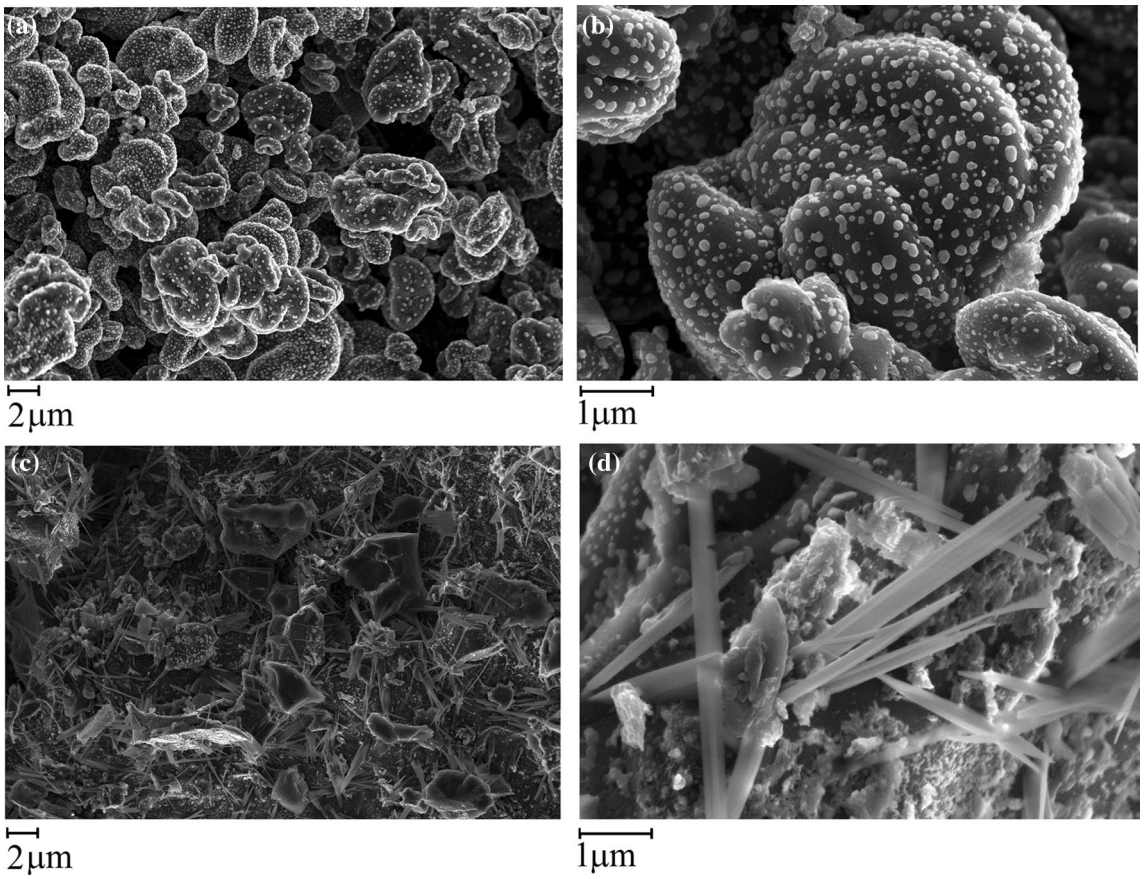

Fig. 7 FE-SEM images of carbonized CNCs EtOH solution at 800 °C (**a** and **b**) and 1000 °C (**c** and **d**)

structures [64]. Material recovered after pyrolysis at 400 °C showed a particular behavior with a 5 wt% loss at 403 °C and a broad curve. This is reasonably due to the high amount of residual functional groups on the surface of carbonaceous materials, as proved by the great fluorescence detected during Raman analysis and bands observed in the FTIR spectrum (Fig. 11b). According to these observations, during the TGA analysis carbonized CNCs completely underwent through pyrolytic degradation forming stable carbon materials in the crucible. Other carbonized CNCs materials showed main degradation process around 500 °C with a decrease in stability observed for those pyrolyzed at 1000 °C. This was in agreement with FESEM analysis that showed a lot of defects onto those structures.

Carbonized solutions of CNCs showed a main degradation stage between 500 and 600 °C. Needle structures obtained using CNCs suspended in water at 800 °C showed an increased stability compared to those produced at 1000 °C. This could be attributable to the defects introduced into the amorphous carbon layers that act as support for the bidimensional carbon structures. Using EtOH solutions, the thermal stability of carbonized CNCs produced at 1000 °C was comparable with material recovered from watery dispersion obtained at 800°. This was in good agreement with FESEM data that showed similar morphologies (Figs. 6c, d, 7c, d). Compared to those produced at 1000 °C, carbonized ethanol CNCs dispersions produced

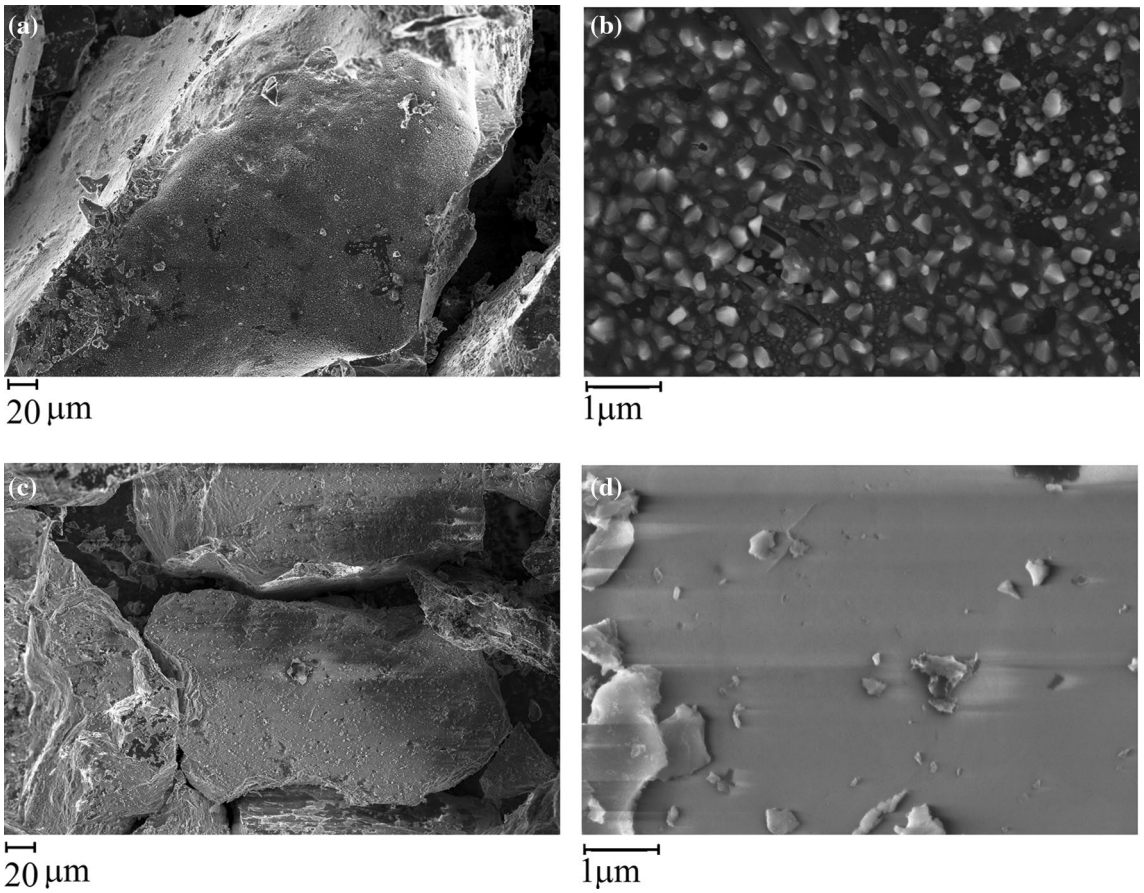

Fig. 8 FE-SEM images of carbonized CNCs PEG solution at 800 °C (**a** and **b**) and 1000 °C (**c** and **d**)

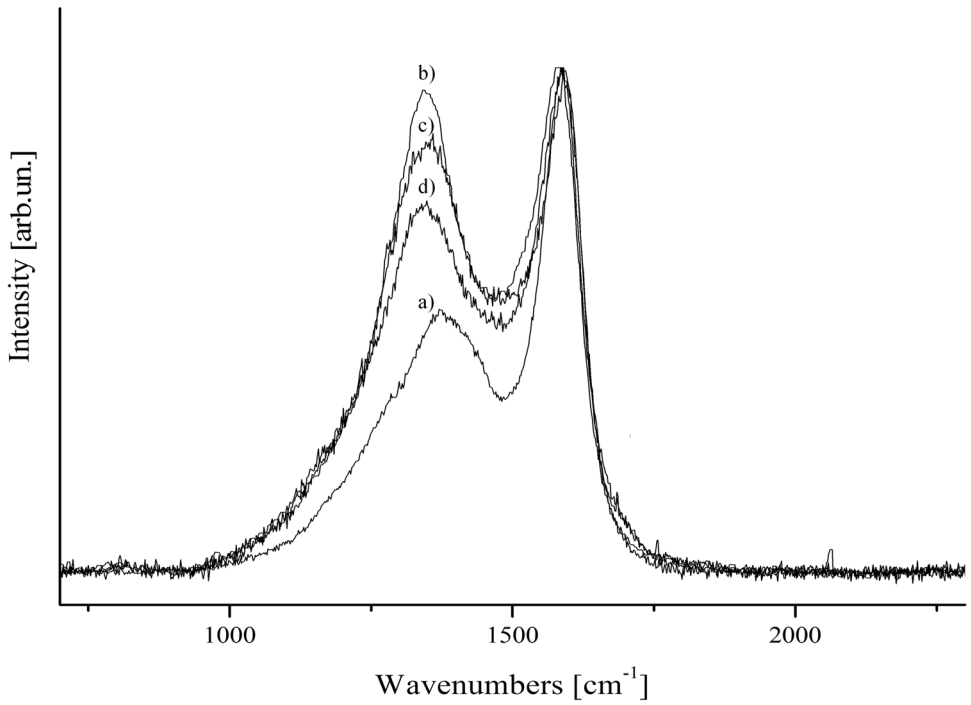

Fig. 9 Raman spectra of carbonized CNCs at HTT of **a** 400 °C, **b** 600 °C, **c** 800 °C and **d** 1000 °C in the region between 700 and 2300 cm^{-1}

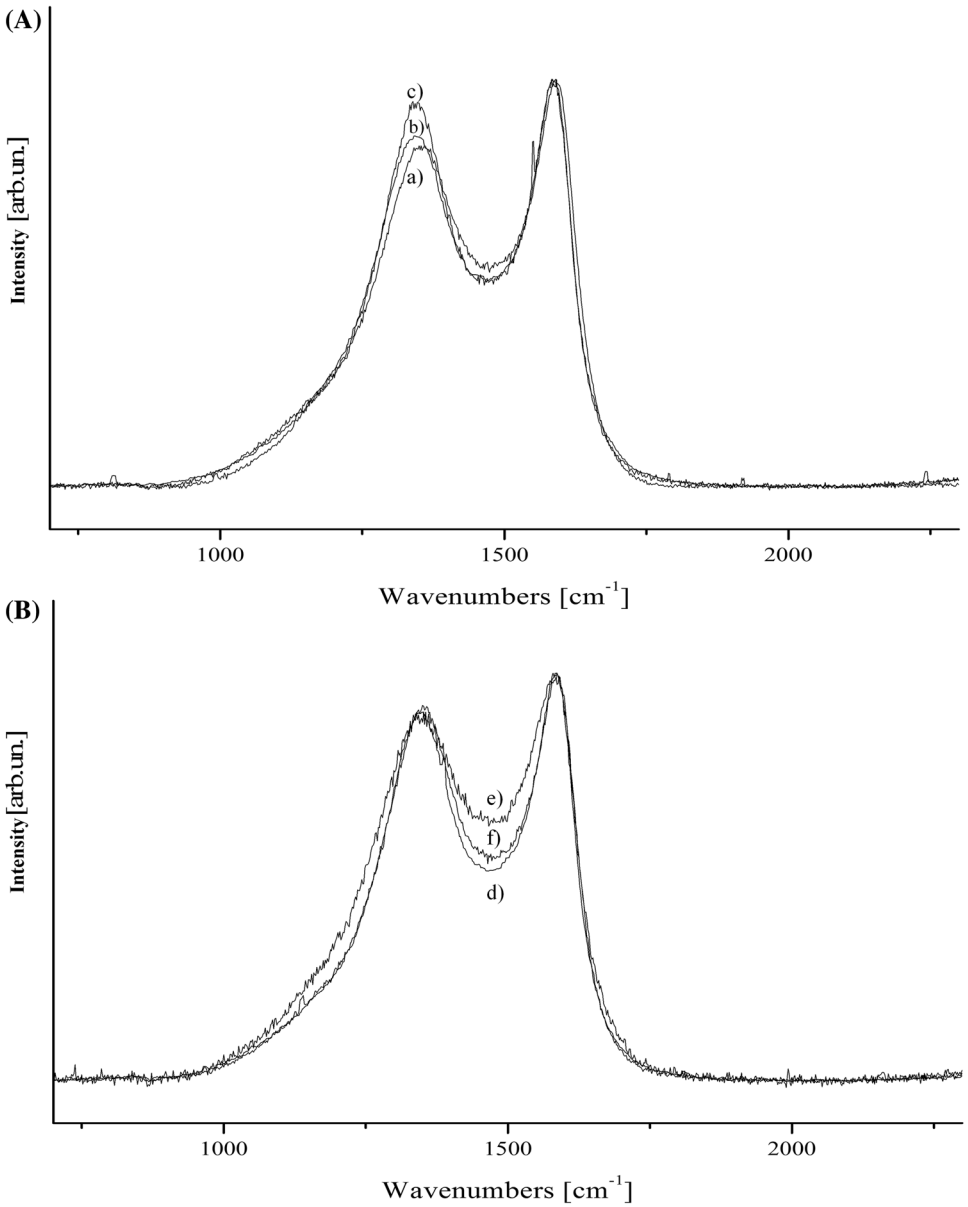

Fig. 10 Raman spectra in the region between 700 and 2300 cm^{-1} of carbonized CNCs solutions at HTT of 800 °C (**A**) using **a** water, **b** EtOH, **c** PEG and at HTT of 1000 °C (**B**) using **d** water, **e** EtOH and **f** PEG

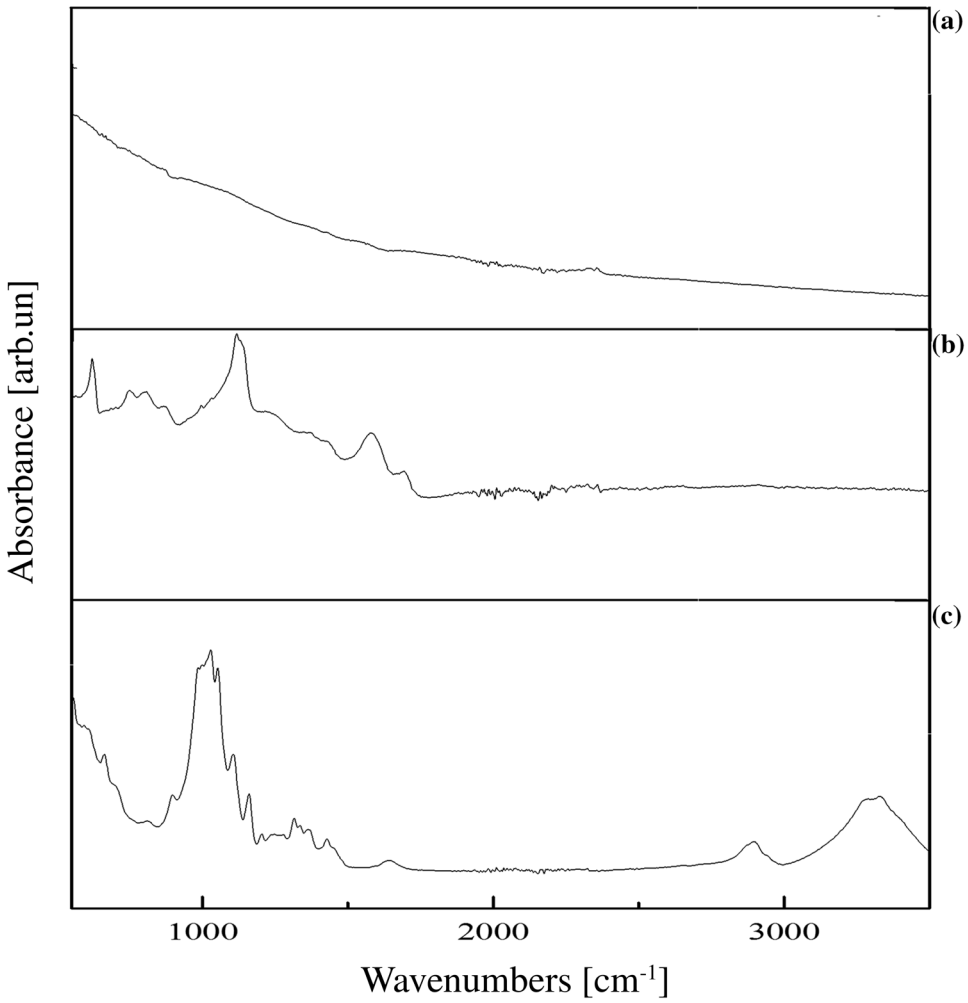

Fig. 11 FT-IR (ATR mode) spectra of carbonized CNCs at **a** 600 °C, **b** 400 °C and **c** solid state form CNCs

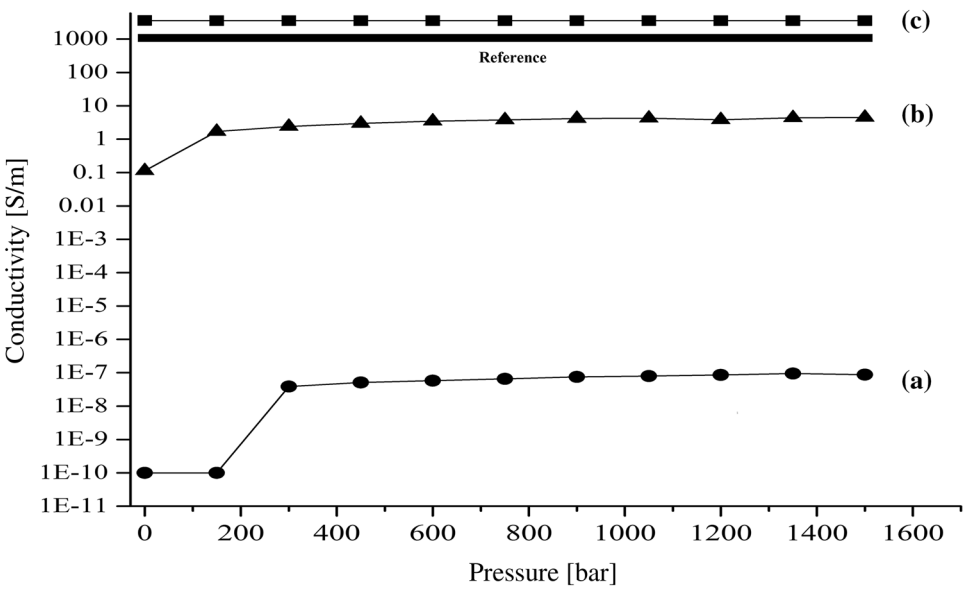

Fig. 12 Relation between pressure and conductivity of carbonized CNCs at **a** 400 °C, **b** 600 °C and **c** copper reference

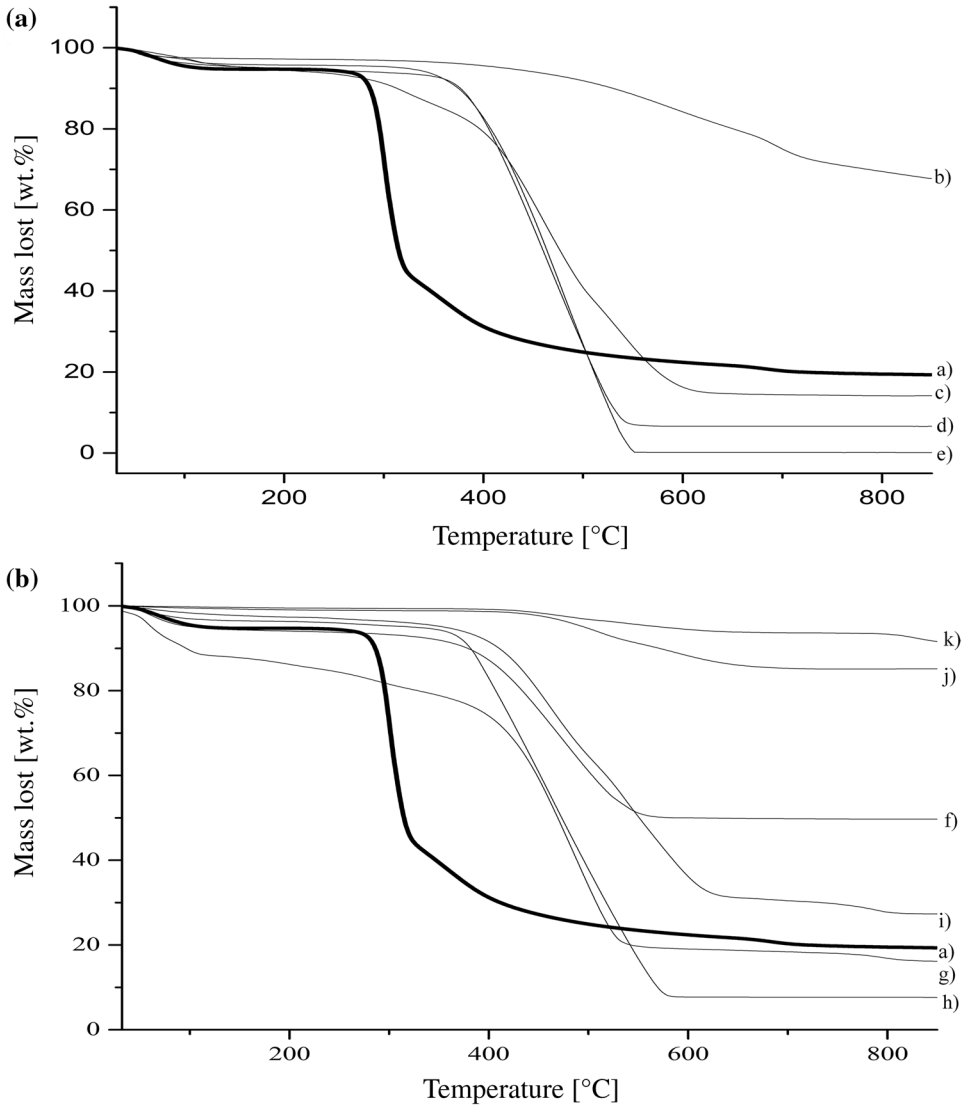

Fig. 13 TGA analysis of **a** pristine CNCs and carbonized CNCs without solvent addition at **b** 400 °C, **c** 600 °C, **d** 800 °C, **e** 1000 °C and using water at **f** 800 °C, **g** 1000 °C, EtOH at **h** 800 °C, **i** 1000 °C and PEG at **j** 800 °C and **k** 1000 °C

at 800 °C were less stable with a broad curve due the thermal decomposition of carbon-on-carbon growth on the surface of CNCs.

A different behavior was observed using CNCs suspended in PEG. In these experiments, the radical-rich environment leads to the formation of more tightly compacted structures (Fig. 8a–d) with an enhanced thermal stability.

4 Conclusions

CNCs were pyrolyzed under different pyrolytic regimes, and carbon-derived materials were analyzed. Increasing temperature from 400 to 1000 °C leads to a drastic increment of conductivity together with the comparison of structural defects such as irregular carbon structures on the surface and the appearance of carbon needles. The use of solvents as dispersing medium induced noteworthy properties to carbonized CNCs. Water promoted the massive formation of carbon needles on amorphous carbon structures at both 800 °C and 1000 °C. The use of EtOH made it possible to switch from carbon-decorated spheres at 800 °C to thin carbon needles at 1000 °C. The use of PEG leads to a richer carbon radical pyrolytic environment inducing the lost of CNCs microstructure. At 800 °C, PEG-dispersed carbonized CNCs were formed by amorphous carbon with tailored nanosized pyramidal structures replaced by smooth surfaces at 1000 °C. The conductivity of carbonized CNCs increased drastically with the temperature, and it was undistinguishable from copper reference passed 800 °C.

Acknowledgements The authors would like to express their acknowledgment and appreciation for the contribution of materials from

Alberta-Pacific Forest Industries and to Salvatore Guastella for FESEM analysis.

Compliance with ethical standards

Conflict of interest The authors declare that they have no conflict of interest.

References

1. Liu C-F, Sun R-C (2010) Chapter 5—cellulose. In: Sun R-C (ed) Cereal straw as a resource for sustainable biomaterials and biofuels. Elsevier, Amsterdam, pp 131–167
2. Silveira MHL, Morais ARC, da Costa Lopes AM, Olekszyszen DN, Bogel-Łukasik R, Andreaus J, Pereira Ramos L (2015) Current pretreatment technologies for the development of cellulosic ethanol and biorefineries. ChemSusChem 8(20):3366–3390
3. Zhang Y-HP (2008) Reviving the carbohydrate economy via multi-product lignocellulose biorefineries. J Ind Microbiol Biotechnol 35(5):367–375
4. Tsao GT, Chou TY (1981) Process for recovering and utilizing cellulose using sulfuric acid. Google patents
5. Dai J, Chae M, Beyene D, Danumah C, Tosto F, Bressler D (2018) Co-production of cellulose nanocrystals and fermentable sugars assisted by endoglucanase treatment of wood pulp. Materials 11(9):1645
6. Brinchi L, Cotana F, Fortunati E, Kenny JM (2013) Production of nanocrystalline cellulose from lignocellulosic biomass: technology and applications. Carbohydr Polym 94(1):154–169. https://doi.org/10.1016/j.carbpol.2013.01.033
7. Trache D, Hussin MH, Haafiz MM, Thakur VK (2017) Recent progress in cellulose nanocrystals: sources and production. Nanoscale 9(5):1763–1786
8. Habibi Y, Lucia LA, Rojas OJ (2010) Cellulose nanocrystals: chemistry, self-assembly, and applications. Chem Rev 110(6):3479–3500
9. Smole MS, Hribernik S, Kurečič M, Krajnc AU, Kreže T, Kleinschek KS (2019) Cellulose nanofibres. In: Navard P (ed) Surface properties of non-conventional cellulose fibres. Springer, Berlin, pp 61–71
10. Aissa K, Karaaslan MA, Renneckar S, Saddler JN (2019) Functionalizing cellulose nanocrystal with click modifiable carbohydrate-binding modules. Biomacromolecules 20:3087–3093
11. Razani S, Tehrani AD (2019) Development of new organic-inorganic, hybrid bionanocomposite from cellulose nanowhisker and Mg/Al-CO_3-LDH for enhanced dye removal. Int J Biol Macromol 133:892–901
12. Borysiak S, Grząbka-Zasadzińska A (2016) Influence of the polymorphism of cellulose on the formation of nanocrystals and their application in chitosan/nanocellulose composites. J Appl Polym Sci 133(3):42864
13. Grząbka-Zasadzińska A, Amietszajew T, Borysiak S (2017) Thermal and mechanical properties of chitosan nanocomposites with cellulose modified in ionic liquids. J Therm Anal Calorim 130(1):143–154
14. Lu Y, Weng L, Cao X (2005) Biocomposites of plasticized starch reinforced with cellulose crystallites from cottonseed linter. Macromol Biosci 5(11):1101–1107
15. Angles MN, Dufresne A (2000) Plasticized starch/tunicin whiskers nanocomposites. 1. Structural analysis. Macromolecules 33(22):8344–8353
16. Lu P, Hsieh Y-L (2010) Preparation and properties of cellulose nanocrystals: rods, spheres, and network. Carbohydr Polym 82(2):329–336
17. Beck S, Bouchard J, Berry R (2012) Dispersibility in water of dried nanocrystalline cellulose. Biomacromolecules 13(5):1486–1494
18. Dubief D, Samain E, Dufresne A (1999) Polysaccharide microcrystals reinforced amorphous poly (β-hydroxyoctanoate) nanocomposite materials. Macromolecules 32(18):5765–5771
19. Chazeau L, Cavaille J, Perez J (2000) Plasticized PVC reinforced with cellulose whiskers. II. Plastic behavior. J Polym Sci Part B Polym Phys 38(3):383–392
20. Peng BL, Dhar N, Liu H, Tam K (2011) Chemistry and applications of nanocrystalline cellulose and its derivatives: a nanotechnology perspective. Can J Chem Eng 89(5):1191–1206
21. da Silva Souza DR, de Mesquita JP, Lago RM, Caminhas LD, Pereira FV (2016) Cellulose nanocrystals: a versatile precursor for the preparation of different carbon structures and luminescent carbon dots. Ind Crops Prod 93:121–128
22. Malik S (1985) Structural and electronic properties of nanocarbon materials such as graphene, nanotubes and fullerenes. Nature 318:162–163
23. Laudenslager MJ, Scheffler RH, Sigmund WM (2010) Electrospun materials for energy harvesting, conversion, and storage: a review. Pure Appl Chem 82(11):2137–2156
24. Tan X, Liu S, Liu Y, Gu Y, Zeng G, Hu X, Wang X, Liu S, Jiang L (2017) Biochar as potential sustainable precursors for activated carbon production: multiple applications in environmental protection and energy storage. Bioresour Technol 227:359–372
25. Mao X, Hatton TA, Rutledge GC (2013) A review of electrospun carbon fibers as electrode materials for energy storage. Curr Org Chem 17(13):1390–1401
26. Wu Q, Li W, Wu Y, Zong G, Liu S (2015) Effect of reaction time on structure of ordered mesoporous carbon microspheres prepared from carboxymethyl cellulose by soft-template method. Ind Crops Prod 76:866–872
27. Zhang X, Li H, Zhang W, Huang Z, Tsui CP, Lu C, He C, Yang Y (2019) In-situ growth of polypyrrole onto bamboo cellulose-derived compressible carbon aerogels for high performance supercapacitors. Electrochim Acta 301:55–62
28. Chen W, Zong Y, Zhou Y, Lu W, Zhang Y, Qian J (2019) The nature of MgO precursor decomposition and pore-forming in hard-templating of porous carbon derived from cotton. Colloids Surf A 571:160–167. https://doi.org/10.1016/j.colsurfa.2019.03.091
29. Wu X, Shi Z, Tjandra R, Cousins AJ, Sy S, Yu A, Berry RM, Tam KC (2015) Nitrogen-enriched porous carbon nanorods templated by cellulose nanocrystals as high performance supercapacitor electrodes. J Mater Chem A 3(47):23768–23777
30. Shopsowitz KE, Hamad WY, MacLachlan MJ (2011) Chiral nematic mesoporous carbon derived from nanocrystalline cellulose. Angew Chem Int Ed 50(46):10991–10995
31. Attia AAM, Antonious MS, Shouman MAH, Nada AAA, Abas KM (2019) Processing and fundamental characterization of carbon fibers and cellulose nanocrystals derived from bagasse. Carbon Lett 29(2):145–154
32. Chang H, Luo J, Liu HC, Zhang S, Park JG, Liang R, Kumar S (2019) Carbon fibers from polyacrylonitrile/cellulose nanocrystal nanocomposite fibers. Carbon 145:764–771
33. Cho SY, Yun YS, Jin H-J (2014) Carbon nanofibers prepared by the carbonization of self-assembled cellulose nanocrystals. Macromol Res 22(7):753–756
34. Eom Y, Son SM, Kim YE, Lee J-E, Hwang S-H, Chae HG (2019) Structure evolution mechanism of highly ordered graphite during carbonization of cellulose nanocrystals. Carbon 150:142–152
35. Meng L, Xu X, Bai B, Ma M, Li S, Hu N, Wang H, Suo Y (2018) Surface carboxyl-activated polyester (PET) fibers decorated with glucose carbon microspheres and their enhanced selective

adsorption for dyes. J Phys Chem Solids 123:378–388. https://doi.org/10.1016/j.jpcs.2018.08.005
36. Wang Y, Cao X, Sun S, Zhang R, Shi Q, Zheng L, Sun R (2019) Carbon microspheres prepared from the hemicelluloses-rich pre-hydrolysis liquor for contaminant removal. Carbohydr Polym 213:296–303. https://doi.org/10.1016/j.carbpol.2019.02.029
37. Liang X, Wen Z, Liu Y, Zhang H, Huang L, Jin J (2011) Highly dispersed sulfur in ordered mesoporous carbon sphere as a composite cathode for rechargeable polymer Li/S battery. J Power Sources 196(7):3655–3658
38. Machado WS, Mamo MA, Coville NJ, Hümmelgen IA (2012) The OFF to ON switching time and ON state consolidation in write-once-read-many-times memory devices based on doped and undoped carbon-sphere/polymer composites. Thin Solid Films 520(13):4427–4431
39. Kim HS, Abbas MA, Kang MS, Kyung H, Bang JH, Yoo WC (2019) Study of the structure–properties relations of carbon spheres affecting electrochemical performances of EDLCs. Electrochim Acta 304:210–220. https://doi.org/10.1016/j.electacta.2019.02.121
40. Ma L, Meng L, Wu G, Wang Y, Zhao M, Zhang C, Huang Y (2015) Effects of bonding types of carbon fibers with branched polyethyleneimine on the interfacial microstructure and mechanical properties of carbon fiber/epoxy resin composites. Compos Sci Technol 117:289–297
41. Shah A, Ding A, Wang Y, Zhang L, Wang D, Muhammad J, Huang H, Duan Y, Dong X, Zhang Z (2016) Enhanced microwave absorption by arrayed carbon fibers and gradient dispersion of Fe nanoparticles in epoxy resin composites. Carbon 96:987–997
42. Giorcelli M, Savi P, Khan A, Tagliaferro A (2019) Analysis of biochar with different pyrolysis temperatures used as filler in epoxy resin composites. Biomass Bioenergy 122:466–471. https://doi.org/10.1016/j.biombioe.2019.01.007
43. Lédé J (2012) Cellulose pyrolysis kinetics: an historical review on the existence and role of intermediate active cellulose. J Anal Appl Pyrol 94:17–32. https://doi.org/10.1016/j.jaap.2011.12.019
44. Ragucci R, Giudicianni P, Cavaliere A (2013) Cellulose slow pyrolysis products in a pressurized steam flow reactor. Fuel 107:122–130. https://doi.org/10.1016/j.fuel.2013.01.057
45. Weber K, Quicker P (2018) Properties of biochar. Fuel 217:240–261
46. Wu J, Wu Z, Tao K, Liu C, Yang B-R, Xie X, Lu X (2019) Rapid-response, reversible and flexible humidity sensing platform using a hydrophobic and porous substrate. J Mater Chem B 7(12):2063–2073
47. Buffa JM, Casado U, Mucci V, Aranguren MI (2019) Cellulose nanocrystals in aqueous suspensions: rheology of lyotropic chiral liquid crystals. Cellulose 26(4):2317–2332
48. Bitounis D, Pyrgiotakis G, Bousfield D, Demokritou P (2019) Dispersion preparation, characterization, and dosimetric analysis of cellulose nano-fibrils and nano-crystals: implications for cellular toxicological studies. NanoImpact 15:100171
49. Börjesson M, Westman G (2015) Crystalline nanocellulose—preparation, modification, and properties. In: Poletto M, Ornaghi HL (eds) Cellulose-fundamental aspects and current trends. InTech, London, pp 159–191
50. Góis GS, Nepomuceno NC, França CH, Almeida YM, Hernandéz EP, Oliveira JE, Oliveira MP, Medeiros ES, Santos AS (2019) Influence of morphology and dispersion stability of CNC modified with ethylene oxide derivatives on mechanical properties of PLA-based nanocomposites. Polym Compos 40(S1):E399–E408
51. Demirbaş A (2005) Thermochemical conversion of biomass to liquid products in the aqueous medium. Energy Sources 27(13):1235–1243
52. Azrina ZZ, Beg MDH, Rosli M, Ramli R, Junadi N, Alam AM (2017) Spherical nanocrystalline cellulose (NCC) from oil palm empty fruit bunch pulp via ultrasound assisted hydrolysis. Carbohydr Polym 162:115–120
53. Iwamoto S, Kai W, Isogai A, Iwata T (2009) Elastic modulus of single cellulose microfibrils from tunicate measured by atomic force microscopy. Biomacromolecules 10(9):2571–2576
54. Uhlig M, Fall A, Wellert S, Lehmann M, Prévost S, Wågberg L, von Klitzing R, Nyström G (2016) Two-dimensional aggregation and semidilute ordering in cellulose nanocrystals. Langmuir 32(2):442–450
55. Undri A, Abou-Zahid M, Briens C, Berruti F, Rosi L, Bartoli M, Frediani M, Frediani P (2015) A simple procedure for chromatographic analysis of pyrolysis bio-oils. J Anal Appl Pyrol 114:208–221. https://doi.org/10.1016/j.jaap.2015.05.019
56. Ferrari AC, Robertson J (2001) Resonant Raman spectroscopy of disordered, amorphous, and diamondlike carbon. Phys Rev B 64(7):075414. https://doi.org/10.1103/PhysRevB.64.075414
57. Ferrari AC, Robertson J (2000) Interpretation of Raman spectra of disordered and amorphous carbon. Phys Rev B 61(20):14095
58. Lu Q, Xiong W-M, Li W-Z, Guo Q-X, Zhu X-F (2009) Catalytic pyrolysis of cellulose with sulfated metal oxides: a promising method for obtaining high yield of light furan compounds. Bioresour Technol 100(20):4871–4876
59. Pang J, Wang A, Zheng M, Zhang T (2010) Hydrolysis of cellulose into glucose over carbons sulfonated at elevated temperatures. Chem Commun 46(37):6935–6937
60. Bartoli M, Rosi L, Giovannelli A, Frediani P, Frediani M (2016) Pyrolysis of a-cellulose in a microwave multimode batch reactor. J Anal Appl Pyrol 120:284–296
61. De Fonton S, Oberlin A, Inagaki M (1980) Characterization by electron microscopy of carbon phases (intermediate turbostratic phase and graphite) in hard carbons when heat-treated under pressure. J Mater Sci 15(4):909–917
62. Downie A, Crosky A, Munroe P (2009) Physical properties of biochar. In: Lehmann J, Joseph S (eds) Biochar for environmental management: science and technology. Earthscan, London, pp 13–32
63. Gabhi RS, Kirk DW, Jia CQ (2017) Preliminary investigation of electrical conductivity of monolithic biochar. Carbon 116:435–442. https://doi.org/10.1016/j.carbon.2017.01.069
64. Mazlan M, Uemura Y, Osman N, Yusup S (2015) Characterizations of bio-char from fast pyrolysis of Meranti wood sawdust. J Phys Conf Ser 1:012054